Electrostatic and magnetostatic properties of random materials

Pouyan Karimi, Xian Zhang, Su Yan, Martin Ostoja-Starzewski, and Jian-Ming Jin

Electrostatic and magnetostatic properties of random materials

Pouyan Karimi[1,2], Xian Zhang[1], Su Yan[2], Martin Ostoja-Starzewski[1,3], Jian-Ming Jin[2]

[1]*Department of Mechanical Science and Engineering,*
[2]*Department of Electrical and Computer Engineering,* [3]*Institute for Condensed Matter Theory,*
University of Illinois at Urbana-Champaign, Urbana, IL 61801, USA
(Dated: January 23, 2019)

Scale dependence of electrostatic and magnetostatic properties is investigated in the setting of spatially random linear lossless materials with statistically homogeneous and spatially ergodic random microstructures. First, from the Hill-Mandel homogenization conditions adapted to electric and magnetic fields, uniform boundary conditions are formulated for a statistical volume element (SVE). From these conditions, there follow upper and lower mesoscale bounds on the macroscale (effective) electrical permittivity and magnetic permeability. Using computational electromagnetism methods, these bounds are obtained through numerical simulations for composites of two types: (i) 2D random checkerboard (two-phase) microstructures and (ii) analogous 3D random (three-phase) media. The simulation results demonstrate a scale-dependent trend of these bounds towards the properties of a representative volume element (RVE). This transition from SVE to RVE is described using a scaling function dependent on the mesoscale δ, the volume fraction v_f, and the property contrast k between two phases. The scaling function is calibrated through fitting the data obtained from extensive simulations ($\sim$10,000) conducted over the aforementioned parameter space. The RVE size of a given microstructure can be estimated down to within any desired accuracy using this scaling function as parametrized by the contrast and the volume fraction of two phases.

I. INTRODUCTION

Multiphase composites can be designed specifically for multifunctional applications to utilize the unique advantages of each phase in the overall, macroscale response. As a result, the effective properties, including electric and magnetic, are affected through the properties of microconstituents, the microstructural geometry, and the scale of observation/resolution. One of the main challenges in the theory of composites lies in homogenization, which is the prediction of macroscopic properties of heterogeneous materials structured in deterministic or random ways. Various models have been used to study the effective properties of heterogeneous composites, see e.g. [1, 2] and references therein. Homogenization of Maxwell's equations has been mostly studied for periodic media; see e.g. [3–6]. In many models of random media, effective properties or bounds are not explicitly scale-dependent, nor is the phase distribution accounted for. For example, simple mixture formulae have been used for non-periodic structures [7]. The objective of this study is to discuss the scale-dependent bounds on the predicted effective electromagnetic parameters of random composites for linear lossless materials at zero frequency.

Assuming a separation of scales, for any given statistically homogeneous and ergodic microstructure, three length scales can be identified - the microscale d (such as the single heterogenity size), the mesoscale L, and the continuum macroscale L_{macro} [8, 9] - satisfying

$$d < L \ll L_{\text{macro}}. \tag{1}$$

In the above, the inequality on the left allows one to postulate the existence of a Representative Volume Element (RVE) of continuum physics. Depending on the geometric randomness and particular properties of the microstructure (especially, the contrast in the material), the RVE may be much larger than the microscale, in which case, $<$ is practically replaced by $\ll$. The inequality $\ll$ on the right allows one to cover the macroscopic length scales up from the RVE (playing the role of a continuum point) where conventional, deterministic continuum physics applies. If a periodic unit cell is assumed, it directly plays the role of RVE. We do not assume any spatial periodicity in our investigation.

In general, L denotes the size of a statistical volume element (SVE), suggesting the basic question: what is the size of RVE, i.e. the scale on which the randomness may be disregarded? In case one wants to work with an SVE, then the resulting continuum model (between the scales L and Lmacro) is stochastic, typically leading to a stochastic partial differential equation (SPDE) on tensor-valued random fields of material properties [10]. This leads to stochastic initial-boundary value problems (IBVPs) on macroscales. If one wants to work with a deterministic continuum model, then the PDE has constant coefficients, leading to deterministic IBVPs on macroscales. The focus of our research is on this SVE-to-RVE scaling, with our strategy proceeding as follows.

First, a macrohomogeneity condition of Hill-Mandel type needs to be formulated [11], [12]. This dictates uniform boundary conditions of either essential or natural types, which, in turn, lead to mesoscale (sometimes called "apparent," as opposed to "effective") material properties of finite-sized domains. Assuming spatial homogeneity and ergodicity of the random medium, upon ensemble averaging, these lead to upper and lower bounds dependent on the type of boundary conditions applied to the domain and the size δ of a mesoscale domain. The latter is the SVE of size L relative to the microscale d, such

as the single grain size. As $\delta = L/d$ increases, the SVE tends towards the RVE on which a homogeneous continuum is being set up, which is the right hand side inequality in Eq. 1. The effective (also called macroscopic or global) property is then determined [9, 13]. Such a scale-dependent homogenization technique has already been employed in many different settings, e.g. thermal conductivity [14], [15], [16], linear or finite elasticity or thermo-elasticity, elasto-plasticity, viscoelasticity, electrical conductivity [17] and permeability [8]. All the linear continuum mechanics/physics problems have been found to share common trends in terms of a scaling function, leading to a question whether they will carry over to electromagnetism.

In the present paper, the above strategy is employed to obtain the SVE-to-RVE scaling for electrostatic and magnetostatic properties of random media, with a numerical illustration for 2D and 3D random checkerboard-type microstructures with zero spatial correlations. The article is organized as follows. The problem formulation including the method used for generating random checkerboards and governing equations is presented in Section II. This is followed by a Hill-Mandel condition for electro- and magneto-static fields and next, in in Section III, by the resulting boundary conditions, the hierarchies of mesoscale bounds, and a formulation of the scaling function. Section IV gives the numerical procedure and results for 2D and 3D systems over a range of parameters and a functional form for the scaling function based on data fitting. The conclusion and major findings are summarized in Section V.

II. PROBLEM FORMULATION

A. Random Microstructure

A dimensionless parameter $\delta = L/d$ is introduced to characterize the mesoscale, where d is the size of a statistically average grain. Next, the mesoscale random material is a set of all the realizations $B_\delta(\omega)$ parametrized by sample events ω in the Ω space

$$\mathbf{B}_\delta = \{B_\delta(\omega); \ \omega \in \Omega\}. \tag{2}$$

Any $B_\delta(\omega)$, while spatially disordered (i.e., heterogeneous), follows the deterministic laws of electromagnetism, see (b) below.

In this article, the spatial (volume-type) averages are denoted by an over-bar ($\bar{\cdot}$), while the statistical (or ensemble) averages are denoted by $\langle \cdot \rangle$. Basically, the microstructure is described by a random (n-component, real valued) field Θ defined over some probability space $\{\Omega, F, P\}$ (with F being a σ-field and P a probability measure) and over some domain $V \in \mathbb{R}^2$ [18]:

$$\mathbf{\Theta} : \Omega \times X \to \mathbb{R}^n. \tag{3}$$

The averages are defined explicitly as

$$\overline{\mathbf{\Theta}(\omega)} = \frac{1}{V} \int_V \mathbf{\Theta}(\omega, \boldsymbol{x}) \, \mathrm{d}V, \qquad \langle \mathbf{\Theta}(\boldsymbol{x}) \rangle = \int_\Omega \mathbf{\Theta}(\omega, \boldsymbol{x}) \, \mathrm{d}P. \tag{4}$$

While the theoretical formulation and strategy outlined in this paper is quite general, all the numerical results are obtained for a so-called random checkerboard (also called random chessboard) in 2D (and 3D), where each square (respectively, cubic) cell of M sites is occupied, independent of the realizations at all other cells, with probabilities p_1 and $p_2 = 1 - p_1$ for phases 1 and 2, respectively. Thus, one cell is the aforementioned grain and, in the language of probability, the random material is a Bernoulli lattice process with a site probability. Clearly, for a square lattice in 2D $L \times L = M$, the number of different realizations is $|\Omega| = 2^{L \times L}$. Given the construction process, each ω occurs with a probability of $1/|\Omega|$. Numerical generation, in a Monte Carlo sense, of such microstructures will be the first step in a computational study of scale-dependent electromagnetic properties.

B. Governing Equations

To set the stage for investigation of the scale-dependent permittivity and permeability, we briefly introduce the basic concepts of electromagnetic theory. We consider every realization $B_\delta(\omega)$ of the random material $\mathbf{B}_\delta$ to be lossless and governed by source-free electro- and magneto-static equations.

Electromagnetism belongs to continuum physics and hence scaling issues analogous to those of physics of other types (e.g., thermoelasticity, elastoplasticity, viscoelasticity...) arise in the context of electromagnetic properties of random heterogeneous materials. The mesoscale (apparent) and macroscale (effective) properties include the electric permittivity ϵ and the magnetic permeability μ. Under the assumption of simple linear media, the constitutive relations that relate the electric field intensity $\mathbf{E}$ with the electric flux density $\mathbf{D}$ and the magnetic field intensity $\mathbf{H}$ with the magnetic flux density $\mathbf{B}$ are [19]

$$\mathbf{D} = \epsilon(\omega, \mathbf{x})\mathbf{E} \tag{5}$$
$$\mathbf{B} = \mu(\omega, \mathbf{x})\mathbf{H}. \tag{6}$$

In any domain of a source-free medium, the electromagnetic fields are governed locally by Maxwell's equations

$$\nabla \times \mathbf{E} = -\mathrm{j}\,(2\pi f)\mu\mathbf{H} \tag{7}$$
$$\nabla \times \mathbf{H} = \mathrm{j}\,(2\pi f)\epsilon\mathbf{E} \tag{8}$$
$$\nabla \cdot \mathbf{D} = 0 \tag{9}$$
$$\nabla \cdot \mathbf{B} = 0 \tag{10}$$

where f is frequency. As the frequency decreases, the coupling between the electric and magnetic fields weakens

and, when the frequency approaches zero ($f \to 0$), the first two equations become

$$\nabla \times \mathbf{E} = 0 \qquad (11)$$

$$\nabla \times \mathbf{H} = 0. \qquad (12)$$

The static electric field $\mathbf{E}$ and static magnetic flux $\mathbf{B}$ can be expressed in terms of the electric scalar potential ϕ and the magnetic vector potential $\mathbf{A}$ as $\mathbf{E} = -\nabla\phi$ and $\mathbf{B} = \nabla \times \mathbf{A}$, respectively.

Let us consider a body $B_\delta(\omega)$ with a given microstructure, in which, as a result of certain boundary conditions and external sources, there are electric and magnetic fields $\mathbf{E}$ and $\mathbf{H}$. We express these fields as superpositions of mean values (indicated by overbars) and zero-mean fluctuations (the primed variables)

$$\mathbf{E}(\omega, \mathbf{x}) = \overline{\mathbf{E}} + \mathbf{E}'(\omega, \mathbf{x}) \qquad (13)$$

$$\mathbf{D}(\omega, \mathbf{x}) = \overline{\mathbf{D}} + \mathbf{D}'(\omega, \mathbf{x}) \qquad (14)$$

$$\mathbf{B}(\omega, \mathbf{x}) = \overline{\mathbf{B}} + \mathbf{B}'(\omega, \mathbf{x}) \qquad (15)$$

$$\mathbf{H}(\omega, \mathbf{x}) = \overline{\mathbf{H}} + \mathbf{H}'(\omega, \mathbf{x}). \qquad (16)$$

Assuming that the domain is the RVE, the effective properties can be defined as

$$\overline{\mathbf{D}} = \epsilon^{\text{eff}}\overline{\mathbf{E}} \qquad (17)$$

$$\overline{\mathbf{B}} = \mu^{\text{eff}}\overline{\mathbf{H}}, \qquad (18)$$

where the randomness (dependence on ω), i.e. the fluctuation, is absent. Also, the response is now independent of the type of boundary conditions, provided that they are uniform; this is explained in more detail below.

III. SCALE-DEPENDENT HOMOGENIZATION: THEORETICAL RESULTS

In this section, a strategy for the problem of size and response of RVE of spatially random linear lossless materials is developed. First, a Hill-Mandel condition for electrostatic and magnetostatic energies is formulated. Then, the bounds of the effective electrical and magnetic properties of random microstructures by means of natural and essential boundary conditions are demonstrated. The convergence of these bounds to the effective properties with increasing length scales is discussed. Finally, the scaling function is formulated as a function of volume fraction, phase contrast, and the mesoscale.

A. Electric Permittivity

The total electrostatic potential energy in terms of the electric field can be expressed in the form $\frac{1}{V}\int_V \mathbf{D} \cdot \mathbf{E}\, dV$. Now, recalling the Hill-Mandel condition for setting up the constitutive equations in micromechanics of solid composite materials [11, 18, 20, 21], by analogy, we set

up an analogous condition for the electrical energy, for any realization $B_\delta(\omega)$,

$$\overline{\mathbf{D} \cdot \mathbf{E}} = \overline{\mathbf{D}} \cdot \overline{\mathbf{E}}. \qquad (19)$$

This means that the energetic interpretation must be equal to the electrical interpretation. Splitting the electric field and flux into their mean and fluctuation parts according to Eqs. (13) and (14), Eq. (19) becomes

$$\overline{(\overline{\mathbf{D}} + \mathbf{D}') \cdot (\overline{\mathbf{E}} + \mathbf{E}')} = \overline{\mathbf{D}} \cdot \overline{\mathbf{E}}. \qquad (20)$$

Since $\overline{\mathbf{D}'} = 0$ and $\overline{\mathbf{E}'} = 0$, Eq. (20) yields

$$\overline{\mathbf{D}' \cdot \mathbf{E}'} = 0. \qquad (21)$$

By analogy to statistics, the spatial averages of the electric flux and electric field may be said to be "spatially uncorrelated".

Now, starting from Eq. (21), it can be shown that

$$
\begin{aligned}
\overline{\mathbf{D}' \cdot \mathbf{E}'} &= \frac{1}{V}\int_V \mathbf{D}' \cdot \mathbf{E}'\, dV \\
&= \frac{1}{V}\int_V (\mathbf{D} - \overline{\mathbf{D}}) \cdot (\mathbf{E} - \overline{\mathbf{E}})\, dV \\
&= \frac{-1}{V}\int_V (\mathbf{D} - \overline{\mathbf{D}}) \cdot (\nabla\phi - \overline{\nabla\phi})\, dV \\
&= -\frac{1}{V}\int_V (\mathbf{D} - \overline{\mathbf{D}}) \cdot [\nabla\phi - \nabla(\overline{\nabla\phi} \cdot \mathbf{x})]\, dV \\
&= -\frac{1}{V}\int_V \nabla \cdot [(\mathbf{D} - \overline{\mathbf{D}})(\phi - (\overline{\nabla\phi} \cdot \mathbf{x}))]\, dV \\
&= -\frac{1}{V}\int_S (\phi - (\overline{\nabla\phi} \cdot \mathbf{x}))[(\mathbf{D} - \overline{\mathbf{D}}) \cdot \mathbf{n}]\, dS \\
&= 0.
\end{aligned}
\qquad (22)
$$

In this derivation, the vector identities $\overline{\nabla\phi} = \nabla(\overline{\nabla\phi} \cdot \mathbf{x})$ and $\nabla \cdot (\phi\mathbf{D}) = \phi(\nabla \cdot \mathbf{D}) + \mathbf{D} \cdot (\nabla\phi)$, the Green-Gauss theorem, and Eq. (9) are used. It follows that Eq. (22) can be satisfied by three different types of uniform boundary conditions on the mesoscale:

(a) the natural (or Neumann, "flux-controlled") boundary condition

$$D_n(x) = D_n^0 \qquad \forall x \in \partial B_\delta; \qquad (23)$$

(b) the essential (or Dirichlet, "potential-controlled") boundary condition

$$\phi(x) = \nabla\phi^0 \cdot \mathbf{x} \qquad \forall x \in \partial B_\delta; \qquad (24)$$

(c) the uniform "mixed-orthogonal" boundary condition

$$[D_n(x) - D_n^0][\phi(x) - \nabla\phi^0 \cdot \mathbf{x}] = 0 \qquad \forall x \in \partial B_\delta. \qquad (25)$$

Here D_n^0 and $\nabla\phi^0$ are employed to denote, respectively, a constant vector and a constant gradient, which are prescribed *a priori*. Each of these boundary conditions results in a different mesoscale (or apparent) permittivity. Since a statistically homogeneous and isotropic random field of electrical properties is assumed, the isotropic response of RVE follows from Eq. (17) as

$$\epsilon^{\text{eff}} = \sqrt{\frac{\overline{\mathbf{D}\cdot\mathbf{D}}}{\overline{\mathbf{E}\cdot\mathbf{E}}}}. \tag{26}$$

B. Magnetic Permeability

The total magnetostatic potential energy in terms of the magnetic field can be expressed in the form $\frac{1}{V}\int_V \mathbf{B}\cdot\mathbf{H}\,\mathrm{d}V$. Following the same strategy as above, the Hill-Mandel condition for magnetic fields leads to

$$\overline{\mathbf{B}'\cdot\mathbf{H}'} = 0. \tag{27}$$

Taking the above equation as the starting point, it can be shown through a similar (but not the same) derivation that

$$
\begin{aligned}
\overline{\mathbf{B}'\cdot\mathbf{H}'} &= \frac{1}{V}\int_V \mathbf{B}'\cdot\mathbf{H}'\,\mathrm{d}V \\
&= \frac{1}{V}\int_V (\mathbf{B}-\overline{\mathbf{B}})\cdot(\mathbf{H}-\overline{\mathbf{H}})\,\mathrm{d}V \\
&= \frac{1}{V}\int_V (\nabla\times\mathbf{A}-\overline{\nabla\times\mathbf{A}})\cdot(\mathbf{H}-\overline{\mathbf{H}})\,\mathrm{d}V \\
&= \frac{1}{V}\int_V [\nabla\times(\mathbf{A}-\tfrac{1}{2}(\overline{\nabla\times\mathbf{A}})\times\mathbf{x})]\cdot(\mathbf{H}-\overline{\mathbf{H}})\,\mathrm{d}V \\
&= \frac{1}{2V}\int_V \nabla\cdot[(\mathbf{A}-(\overline{\nabla\times\mathbf{A}})\times\mathbf{x})\times(\mathbf{H}-\overline{\mathbf{H}})]\,\mathrm{d}V \\
&= \frac{1}{2V}\int_S [(\mathbf{A}-(\overline{\nabla\times\mathbf{A}})\times\mathbf{x})\times(\mathbf{H}-\overline{\mathbf{H}})]\cdot\mathbf{n}\,\mathrm{d}S \\
&= 0.
\end{aligned}
\tag{28}
$$

In the above, the vector identities $\overline{\mathbf{B}} = \frac{1}{2}\nabla\times(\overline{\mathbf{B}}\times\mathbf{x})$ and $\nabla\cdot(\mathbf{A}\times\mathbf{H}) = (\nabla\times\mathbf{A})\cdot\mathbf{H}-\mathbf{A}\cdot(\nabla\times\mathbf{H})$, the Green-Gauss theorem, and Eq. (12) are used. Clearly, Eq. (28) can be satisfied by three different types of uniform boundary conditions on the mesoscale:

(a) the natural (Neumann, "current-controlled") boundary condition

$$\mathbf{n}\times\mathbf{H} = \mathbf{n}\times\mathbf{H}^0 \qquad (\mathbf{J}_s = \mathbf{J}_s^0) \qquad \forall x\in\partial B_\delta; \tag{29}$$

(b) the essential (Dirichlet, "potential-controlled") boundary condition

$$\mathbf{n}\times\mathbf{A} = \mathbf{n}\times[(\nabla\times\mathbf{A}^0)\times\mathbf{x}] \qquad \forall x\in\partial B_\delta; \tag{30}$$

(c) the uniform "mixed-orthogonal" boundary condition

$$[\,\mathbf{n}\times\mathbf{H}-\mathbf{n}\times\mathbf{H}^0\,]\cdot[\,\mathbf{n}\times\mathbf{A}-\mathbf{n}\times[(\nabla\times\mathbf{A}^0)\times\mathbf{x}]\,] = 0$$
$$\forall x\in\partial B_\delta. \tag{31}$$

Again, since a statistically homogeneous and isotropic random field of magnetic properties is assumed, the isotropic response of the RVE is calculated using Eq. (18) as

$$\mu^{\text{eff}} = \sqrt{\frac{\overline{\mathbf{B}\cdot\mathbf{B}}}{\overline{\mathbf{H}\cdot\mathbf{H}}}}. \tag{32}$$

Note that, for 2D cases, since the magnetic field is in the xy plane, $\mathbf{A}$ has the z component only. It can be shown that, for the 2D magneto-static case, the governing equation is simplified to

$$\nabla\cdot\left(\frac{1}{\mu}\nabla A_z\right) = -J_z, \tag{33}$$

where J_z is the impressed current source in the z direction. This is similar to the governing equation for the electro-static case $\nabla\cdot(\epsilon\nabla\phi) = -\rho$ with ρ being the impressed charge. Therefore, there is a duality between boundary conditions for the electro- and magneto-static cases:

$$\nabla\cdot(\epsilon\nabla\phi) = -\rho \Rightarrow \begin{cases} D_n = D_n^0 \quad (\rho=\rho^0) \\ \phi = \nabla\phi^0\cdot\mathbf{x}, \end{cases} \tag{34}$$

$$\nabla\cdot\left(\frac{1}{\mu}\nabla A_z\right) = -J_z \Rightarrow \begin{cases} J_z = J_z^0 \\ A_z = (\nabla\times\mathbf{A}^0)\times\mathbf{x}. \end{cases} \tag{35}$$

It should be noted that besides the vector magnetic potential $\mathbf{A}$, a magnetic scalar potential ϕ_m can also be used. In that case, the governing equation (33) and the boundary conditions (34-35) are replaced by

$$\nabla\cdot(\mu\nabla\phi_m) = -\rho_m \Rightarrow \begin{cases} B_n = B_n^0 \quad (\rho_m=\rho_m^0) \\ \phi_m = \nabla\phi_m^0\cdot\mathbf{x} \end{cases} \tag{36}$$

where ρ_m is the impressed magnetic charge.

The fact that the random sample must be large enough to have relatively small boundary field fluctuations relative to its size and, simultaneously, be small enough relative to a macroscopic structure of scale L_{macro} in Eq. (1), forces us to consider the responses stemming from the various boundary conditions in more detail.

C. Hierarchies of Mesoscale Bounds in Electro-/Magneto-Static Cases

Since the gradient is prescribed in the essential (^{e}) boundary condition (24) of the electrostatic problem of

any realization $B_\delta(\omega)$, it results in a *mesoscale* permittivity tensor $\epsilon_\delta^e(\omega)$. However, since the current is prescribed in the natural $(^n)$ boundary condition (23), it yields a *mesoscale* resistivity tensor $\mathbf{s}_\delta^n(\omega)$. [We borrow the terminology "resistivity" from conductvity phenomena because there is no corresponding term.] Finally, the mixed $(^m)$ boundary condition (25) results in a *mesoscale* permittivity tensor $\epsilon_\delta^m(\omega)$ or, depending on the interpretation, resistivity $\mathbf{s}_\delta^m(\omega)$. The argument ω explicitly indicates the random character of these tensors, while δ indicates their scale dependence, so that these tensors pertain to the statistical volume element (SVE) responses.

The randomness vanishes as $\delta \to \infty$, and this is the *macroscale* response C_∞ of a representative volume element (RVE), where a deterministic continuum picture is obtained.

By reference to variational principles of electromagnetism, all these tensors are positive-definite and satisfy an ordering relation

$$[\mathbf{s}_\delta^n(\omega)]^{-1} \le \epsilon_\delta^m(\omega) \le \epsilon_\delta^e(\omega). \qquad (37)$$

The inequalities are understood in the same sense as in the definition of positive-definiteness: if $\mathbf{A}$ and $\mathbf{B}$ are the rank 2 tensors, then $\mathbf{A} \le \mathbf{B}$ means $\mathbf{v} : \mathbf{A} : \mathbf{v} \le \mathbf{v} : \mathbf{B} : \mathbf{v}$, for any rank 1 tensor $\mathbf{v}$. From the above we obtain a relation between the ensemble averages: $\langle \mathbf{s}_\delta^n \rangle^{-1} \le \langle \epsilon_\delta^m \rangle \le \langle \epsilon_\delta^e \rangle$. The response $\langle \epsilon_\delta^m \rangle$ displays a much weaker scaling than the other two; it will not be pursued because, in contradistinction to $\langle \mathbf{s}_\delta^n \rangle^{-1}$ and $\langle \epsilon_\delta^e \rangle$, it does not have a bounding property.

Using the variational principles for boundary value problems under (23) and (24) in combination with the assumption of spatial homogeneity and ergodicity of random microstructure, one arrives at the result that, the larger is the mesoscale material domain B_δ, the 'softer' is $\langle \epsilon_\delta^e \rangle$ and the 'stiffer' is $\langle \mathbf{s}_\delta^n \rangle^{-1}$. This is analogous to the scaling of bounds from displacement and traction loadings in elasticity of random media [8, 18, 20]. Combining these results, we have a hierarchy of scale-dependent bounds on the RVE response ϵ_∞:

$$\langle \mathbf{s}_1^n \rangle^{-1} \le \langle \mathbf{s}_{\delta'}^n \rangle^{-1} \le \langle \mathbf{s}_\delta^n \rangle^{-1} \le \epsilon_\infty \le \langle \epsilon_\delta^e \rangle \le \langle \epsilon_{\delta'}^e \rangle \le \langle \epsilon_1^e \rangle$$
$$\forall \delta' < \delta. \quad (38)$$

On account of the spatial homogeneity and ergodicity of the material, the tensor ϵ_∞ is identified with the so-called effective ϵ^{eff}. By reference to continuum micromechanics, in (38) we also recognize the Reuss-type bound $(\mathbf{s}^R = \langle \mathbf{s}_1^n \rangle^{-1})$ and the Voigt-bound bound $(\epsilon^V = \langle \epsilon_1^e \rangle)$, which clearly possess no scale dependence.

All the above developments carry over to the magneto-static problem, where ϵ (or ϵ) is replaced with μ (or μ). In fact, Fig. 1 depicts the corresponding hierarchies obtained for random checkerboards.

D.   Formulation of Scaling Function

Suppose we deal with a random polycrystal. In general, for any given realization $B_\delta(\omega)$ of $\mathbf{B}_\delta(\omega)$, $\epsilon_\delta^e(\omega)$ and $\mathbf{s}_\delta^n(\omega)$ are anisotropic. A statistically isotropic response applies if all the crystal orientations are uniformly distributed on a unit sphere, while a deterministically isotropic response is obtained upon ensemble averaging on any mesoscale. Thus, we have

$$\langle \mathbf{s}_\delta^n \rangle = s_\delta^n \mathbf{I}, \quad \epsilon_\infty = \epsilon_\infty \mathbf{I}, \quad \epsilon_\delta = \epsilon_\delta^e \mathbf{I}. \qquad (39)$$

where $\mathbf{I}$ is the rank 2 identity tensor. From the above, we obtain

$$\langle \mathbf{s}_\delta^n \rangle : \langle \epsilon_\delta^e \rangle = D \, \epsilon_\delta^d \, s_\delta^n, \qquad (40)$$

where D is the dimensionality of space, i.e. either 2 or 3. In the infinite volume limit ($\delta \to \infty$ on the RVE level), one tensor is the exact inverse of another

$$\lim_{\delta \to \infty} \langle \mathbf{s}_\delta^n \rangle : \langle \epsilon_\delta^e \rangle = D. \qquad (41)$$

Also in the case of statistically isotropic statistics, there holds a special case of hierarchy of bounds (38) on ϵ_∞ in (39):

$$s^R \le \langle s_{\delta'}^n \rangle^{-1} \le \langle \epsilon_\delta^n \rangle^{-1} \le \epsilon_\infty \le \langle \epsilon_\delta^e \rangle \le \langle \epsilon_{\delta'}^e \rangle \le \epsilon^V,$$
$$\forall \delta' < \delta. \quad (42)$$

With each crystal's conductivity being characterized by three principal values $(c_1, c_2, c_3,)$, the Reuss-type and Voigt-type bounds are $s^R = [(1/\epsilon_1 + 1/\epsilon_2 + 1/\epsilon_3)/3]^{-1}$ (harmonic) and $\epsilon^V = (\epsilon_1 + \epsilon_2 + \epsilon_3)/3$ (arithmetic), respectively.

Focusing on the 2D case, we set up the following relationship between the left hand sides of (40) and (41):

$$\langle \epsilon_\delta^e \rangle : \langle \mathbf{s}_\delta^n \rangle = \lim_{\delta \to \infty} \langle \epsilon_\delta^e \rangle : \langle \mathbf{s}_\delta^n \rangle + g(\delta, v_f, k) \qquad (43)$$

where $f(\delta, v_f, k)$ defines the *scaling function*, with the volume fraction v_f of phase 2, and the contrast $k = \epsilon_1/\epsilon_3$ being a non-dimensional parameter. Also, from the above equations

$$f(\delta, v_f, k) = 2\left(\epsilon_\delta^e \, s_\delta^n - 1\right), . \qquad (44)$$

The scaling function has the property: $f(\delta \to \infty, v_f, k) = f(\delta, v_f, k = 1) = 0$; the latter is the case of crystals being locally isotropic with $k = 1$ (such as for cubic crystals).

Again, all the above developments carry over to the magneto-static problem, where ϵ (or ϵ) is replaced with μ (or μ).

IV.   NUMERICAL RESULTS

The electro- and magneto-static behaviors of planar random checkerboard are simulated by the finite element method (FEM) using COMSOL Multiphysics via
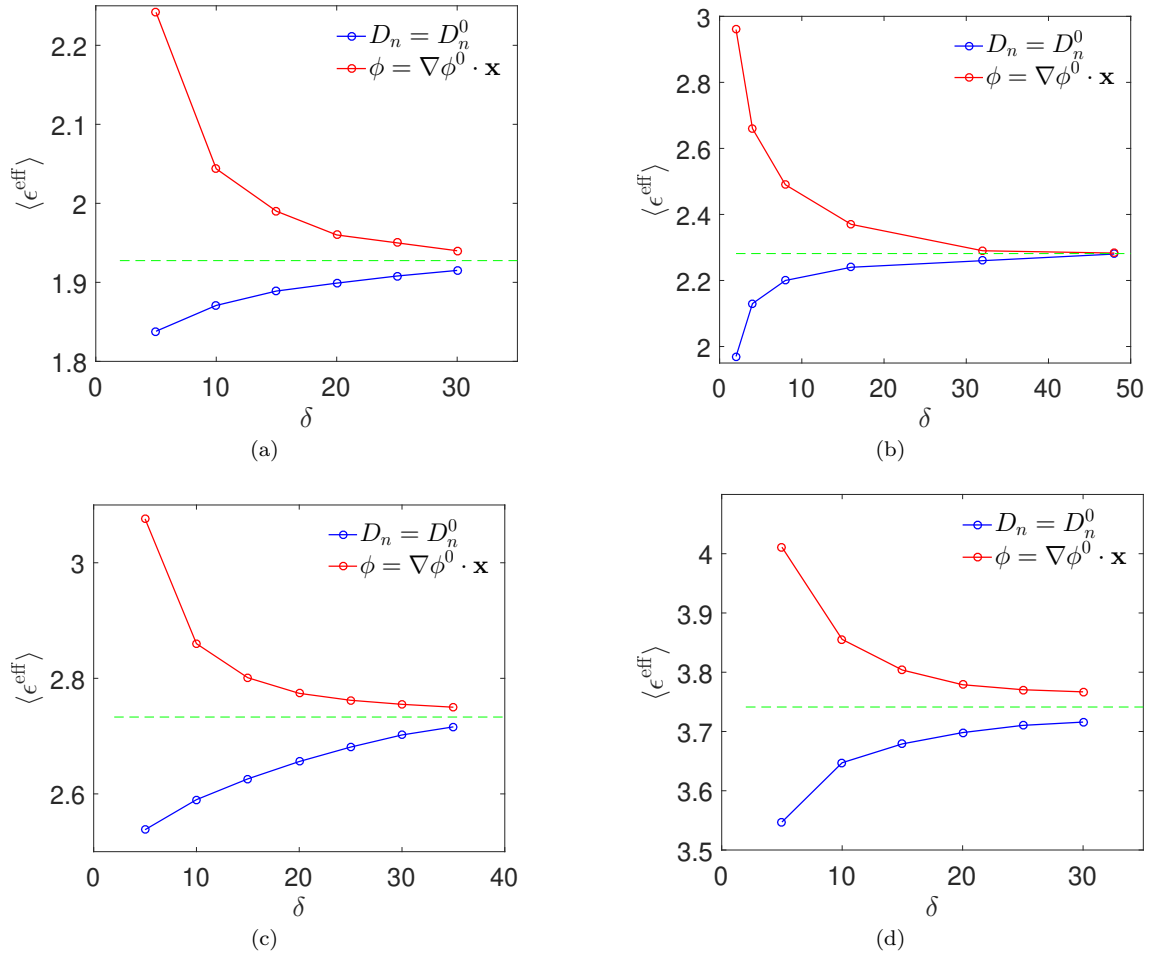
FIG. 1: (Color online) Mesoscale bounds on effective (i.e., macroscopic) permittivity of random checkerboards with increasing volume fraction of second phase (a) $v_f = 0.4$, (b) $v_f = 0.5$, (c) $v_f = 0.6$, and (d) $v_f = 0.8$ for $\epsilon_1 = 1$ and $\epsilon_2 = 5$.

Livelink for MATLAB, a commercial FEM solver [22]. The mesh density is important especially for higher values of k where the interface between two phases has a jump in the permittivty (or permeability) value. Olariu et al. [23] conducted a comprehensive analysis of influence of high contrast on the numerically estimated effective permittivity. With an increasing contrast k, at a given size and mesh density, a greater error is expected in numerically estimated effective properties. Thus, to have an acceptable accuracy and capture the strong gradients, a finer mesh is needed for a stronger contrast.

For a given realization $B_\delta(\omega)$ with volume fraction v_f and contrast k, the mesoscale permittivity $\boldsymbol{\epsilon}_\delta^n$ and $\boldsymbol{\epsilon}_\delta^e$ will now be determined using Eqs. (23) and (24), respectively. First, $\boldsymbol{\epsilon}_\delta^n$, a constant normal electric displacement D_n^0 is applied on the boundaries of the domain and the volume average electric field $\overline{\mathbf{E}}$ and $\overline{\mathbf{D}}$ are calculated from the numerical solution obtained. Then using Eq. (26), the mesoscale permittivity $\boldsymbol{\epsilon}_\delta^n$ is evaluated. To get $\boldsymbol{\epsilon}_\delta^e$, a constant potential gradient $\nabla\phi^0$ is applied on the boundaries and the volume averaged $\overline{\mathbf{E}}$ and $\overline{\mathbf{D}}$ are obtained using the numerical values. Then, the mesoscale permittivity ϵ_δ^e is evaluated using Eq. (26).

Note that the mesoscale permittivity tensor is, in general, anisotropic for any realization at any mesoscale δ. However, if the random field is statistically isotropic, the statistically averaged permittivity tensor is isotropic, i.e., it is approximately isotropic in the Monte Carlo sampling.

The mesoscale bounds of permittivity are plotted as functions of δ in Fig. 1 when volume fraction of phase 2 is $v_f = \{0.4, 0.5, 0.6, 0.8\}$. The relative permittivities of phase 1 and phase 2 are $\{1, 5\}$ ($k = 5$), respectively. For each δ, at least one hundred realizations are simulated, and the ensemble average is reported.

For a given realization $B_\delta(\omega)$ with volume fraction v_f and contrast k, the mesoscale permeability μ_δ^n and μ_δ^e can be calculated using Eqs. (29) and (30), respectively. For the mesoscale μ_δ^n, a constant surface current J_z^0 is applied on the boundaries of the domain and the volume averaged magnetic field $\overline{\mathbf{H}}$ and magnetic flux $\overline{\mathbf{B}}$ are calculated from the numerical solution. Then, using Eq. (32), the mesoscale permeability μ_δ^n is evaluated. To obtain μ_δ^e, a constant potential $(\nabla \times A_z^0)$ is applied on the boundaries, resulting in volume averaged $\overline{\mathbf{H}}$ and $\overline{\mathbf{B}}$. Then, using Eq. (32), the mesoscale permeability μ_δ^e is evaluated.

The mesoscale bounds of permeability are plotted as functions of δ in Fig. 2 and Fig. 3 when the volume fraction, v_f, of phase 2 is $\{0.5, 0.8\}$. The relative permeabilities of phase 1 and phase 2, respectively, are $\{1, 3\}$ and $\{1, 7\}$. For each δ, at least one hundred realizations are simulated, and the statistical average is reported.

Figure 4 depicts the magnetic flux norm and magnetic field norm of the two-phase random checkerboard for $L = 16$ with $v_f = 0.5$ under the boundary condition $(\nabla \times A_z^0) \times \mathbf{x}$.

It should be noted that for any given realization at a finite mesoscale δ the mesoscale permittivity or perme-

ability tensors need not be isotropic, i.e., the values in x and y directions can be different. As mentioned before, the entire formulation discussed in the previous sections, without any limitation, can be applied to 3D cases and/or anisotropic medium whose $\boldsymbol{\epsilon}$ and $\boldsymbol{\mu}$ are tensors. For an anisotropic medium, the constitutive relations cannot be expressed in a simple form as in Eq. (17). Instead, they have to be expressed as

$$\begin{cases} \mathbf{D} = \bar{\bar{\boldsymbol{\epsilon}}} \cdot \mathbf{E} \\ \mathbf{B} = \bar{\bar{\boldsymbol{\mu}}} \cdot \mathbf{H} \end{cases} \tag{45}$$

where $\bar{\bar{\boldsymbol{\epsilon}}}$ and $\bar{\bar{\boldsymbol{\mu}}}$ are called permittivity and permeability tensors. Crystals are a special case of general anisotropic media, which have a diagonal permittivity tensor. Here, biaxial media which have diagonal permittivity tensors with different values are considered [19]. If statistically homogeneous random fields of electrical and magnetic properties are assumed, the isotropic response of RVE can be calculated using Eq. (45) as

$$\epsilon_{xx}^{\text{eff}} = \sqrt{\frac{\overline{\mathbf{D}_x \cdot \mathbf{D}_x}}{\overline{\mathbf{E}_x \cdot \mathbf{E}_x}}}, \qquad \epsilon_{yy}^{\text{eff}} = \sqrt{\frac{\overline{\mathbf{D}_y \cdot \mathbf{D}_y}}{\overline{\mathbf{E}_y \cdot \mathbf{E}_y}}}. \tag{46}$$

The mesoscale permittivity bounds obtained for x and y directions of two biaxial phases with $v_f = 0.5$ are shown in Fig. 5. The relative permittivity tensors for the first and second phases, respectively, are $\begin{bmatrix} 2 & 0 \\ 0 & 4 \end{bmatrix}$ and $\begin{bmatrix} 4 & 0 \\ 0 & 7 \end{bmatrix}$.

The geometry and corresponding electric field norm of one realization of the 3D material (for $\epsilon = \{1, 10\}$ with $v_f = 0.5$) under the boundary condition $\nabla\phi^0 = 10$ are depicted in parts (a) and (b) of Fig. 6; the latter figure is taken from a 3D animation, attached in GIF format [24]. In part (c) we see the mesoscale permittivity bounds for this 3D case as well as for a completely analogous 2D random material with all physical parameters kept the same. This gives a comparison of scaling trends: evident here is the much more rapid trend to homogenize, as the mesoscale increases, of the 3D random material as compared to situation of the 2D material. This may be explained qualitatively by a reference to the 3D Green's function $\dfrac{1}{r}$ as opposed to the 2D Green's function $\dfrac{1}{\sqrt[2]{r}}$.

A 3d movie showing a perspective view of the field of electric flux density norm, whose snapshot is in Fig. 5(b), is found in the Electronic Supplementary Material.

Following the study in [9], the scaling function for a two-phase random checkerboard can be written as the product of the material-dependent and the scale-dependent quantities

$$f\left(\delta, v_f, k\right) = 2\left(\epsilon_\delta^e \ s_\delta^n - 1\right) g(\delta)$$
$$= 2v_f\left(1 - v_f\right)\left(\sqrt{k} - \frac{1}{\sqrt{k}}\right)^2 g(\delta) \tag{47}$$

where $g(\delta)$ defines the normalized scaling function, which depends exclusively on the mesoscale. Inspired by the
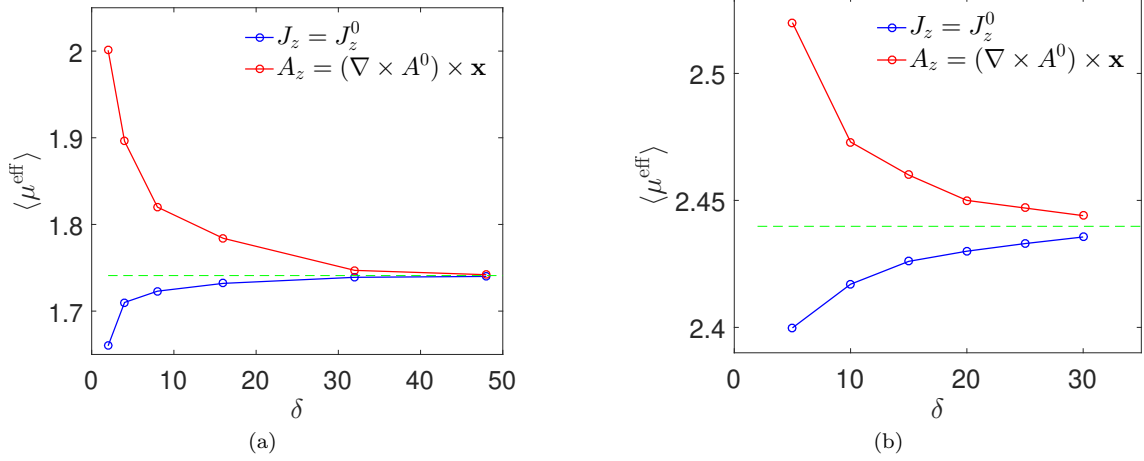
(a)

(b)

FIG. 2: (Color online) Mesoscale bounds on effective (i.e., macroscopic) permeability of a random checkerboard with increasing volume fraction of second phase (a) $v_f = 0.5$ and (b) $v_f = 0.8$ for $\mu_1 = 1$ and $\mu_2 = 3$.
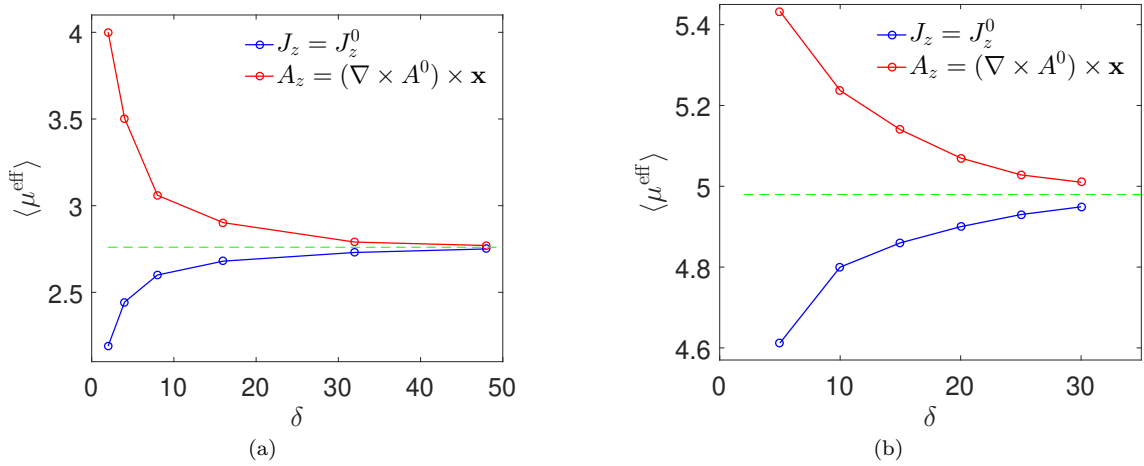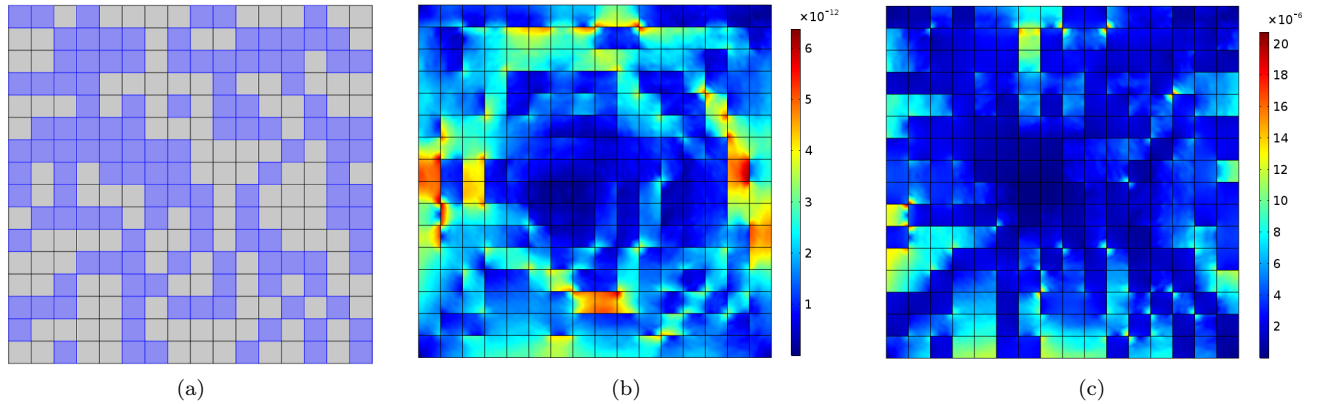

(a)

(b)

FIG. 3: (Color online) Mesoscale bounds on effective (i.e., macroscopic) permeability of a random checkerboard with increasing volume fraction of second phase (a) $v_f = 0.5$ and (b) $v_f = 0.8$ for $\mu_1 = 1$ and $\mu_2 = 7$.

(a)

(b)

(c)

FIG. 4: (Color online) (a) Realization of a two phase random checkerboard for $L = 16$. (b) Magnetic flux norm density (T). (c) Magnetic field norm (A/m).
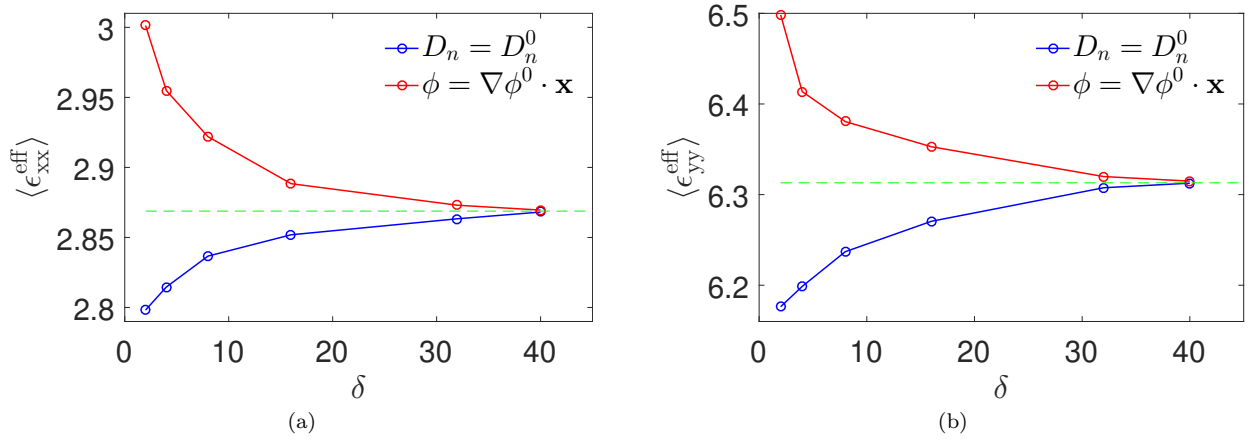
FIG. 5: (Color online) Mesoscale bounds on effective (i.e., macroscopic) permittivity of a random checkerboard in (a) x direction and (b) y direction with $v_f = 0.5$.
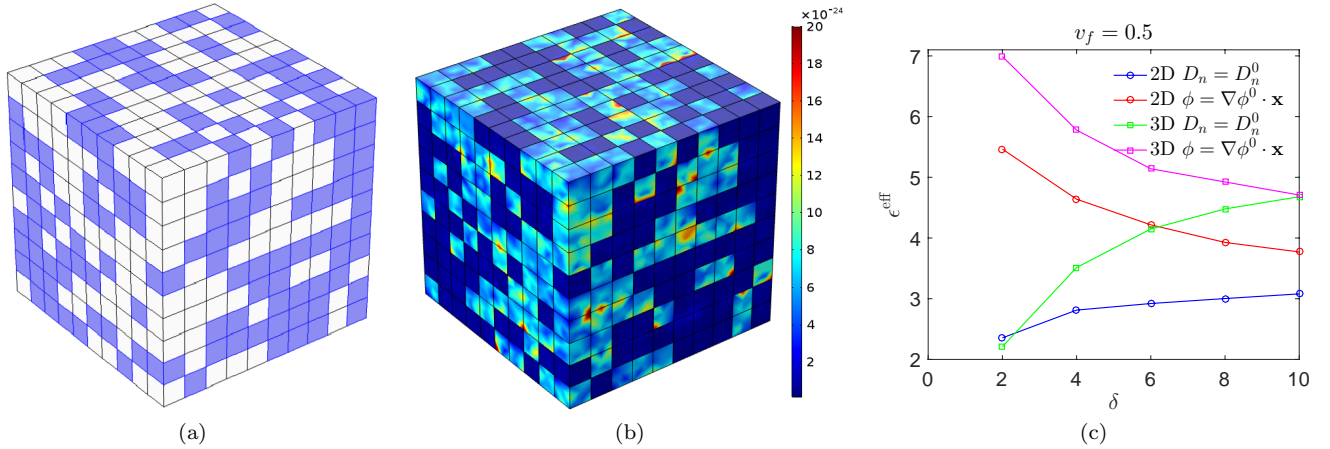

FIG. 6: (Color online) Two-phase random checkerboard for $\epsilon = \{1, 10\}$ and $v_f = 0.5$. (a) 3D two-phase random checkerboard on the $L \times L \times L$ lattices with $L = 10$. (b) Electric flux density norm $(\mathrm{C/m^2})$ for 3D two-phase random checkerboard, taken from the attached animation. (c) Comparison of scaling effects for $v_f = 0.5$ in 2D and 3D random two phase checkerboard.

study conducted in [9], the following stretched exponential fit of the normalized scaling function is employed

$$g(\delta) = \exp\left[A(\delta - 1)^B\right]. \qquad (48)$$

Figure 7a shows the normalized scaling function obtained for $v_f = 0.5$ and $k = \{3, 5, 7\}$ with fitting constants $A = 0.73 \pm 0.03$ and $B = 0.5 \pm 0.02$. It is interesting to see that the dependence of material contrast (k) can be removed by normalizing the scaling function with $\left(\sqrt{k} - \frac{1}{\sqrt{k}}\right)^2$.

Figure 7b shows the normalized scaling function obtained for $k = 7$ and $v_f = \{0.2, 0.4, 0.6, 0.8\}$ with fitting constants $A = 0.73 \pm 0.03$ and $B = 0.5 \pm 0.01$. It is interesting to see that the dependence of volume fraction (v_f) can be removed by normalizing the scaling function with $2v_f (1 - v_f)$. From Figs. 7a and 7b, it is clear that $\delta = 30$ is large enough to be accepted as the RVE size.

Effectively, the mesoscale (δ) dependence of the random checkerboard microstructure for any combination of k and v_f can be explained by the normalized scaling function $g(\delta)$. It should be noted that the scale dependency of scaling function for permittivity (or permeability) only shows the rate of convergence to RVE, and has nothing to do with the effective property. However, for a sufficiently large δ, it provides bounds which are tight enough to estimate the effective property with very good accuracy.

V. CONCLUSION

In this article, a methodology to study the length scale effect on the permittivity and permeability of random checkerboard composites is proposed within the framework dictated by the Hill-Mandel condition. The responses from two stochastic initial boundary value problems bound the permittivity and permeability from above and below, respectively, for essential and natural boundary conditions. Finite element simulations are employed to illustrate the results of random checkerboards with varying phase contrasts at arbitrary nominal volume fractions. Hierarchies of mesoscale bounds are also discussed. This method can be employed to assess the passage from SVE-to-RVE for a random material with linear lossless, perfectly bounded microconstituents.

The convergence to the effective medium response can be predicted for other combinations of microconstituents' properties and other microstructural geometries using a scalar-valued scaling function. Numerical simulations are employed to construct its functional form as a function of the volume fraction, phase contrast, and the mesoscale. Its effectiveness in grasping the scaling properties is also studied.

While the numerical examples are carried out for planar random checkerboard morphologies, the entire methodology is also applicable to other 2D or 3D systems of spatially correlated geometries [10], providing their spatial statistics are homogeneous and ergodic. However,

the longer-range are the correlations of phase distributions, the slower is the SVE-to-RVE scaling trend and, necessarily, the larger are the mesoscale volumes needed for simulation. Also, while the present report is limited to linear and lossless media, this methodology can be extended to homogenization of nonlinear and lossy media.

The reported work is now being used as a stepping-stone for analysis of electromagnetic properties in the frequency domain (including a generalization of scaling laws such as Eqs. (47-48), as will be reported separately.
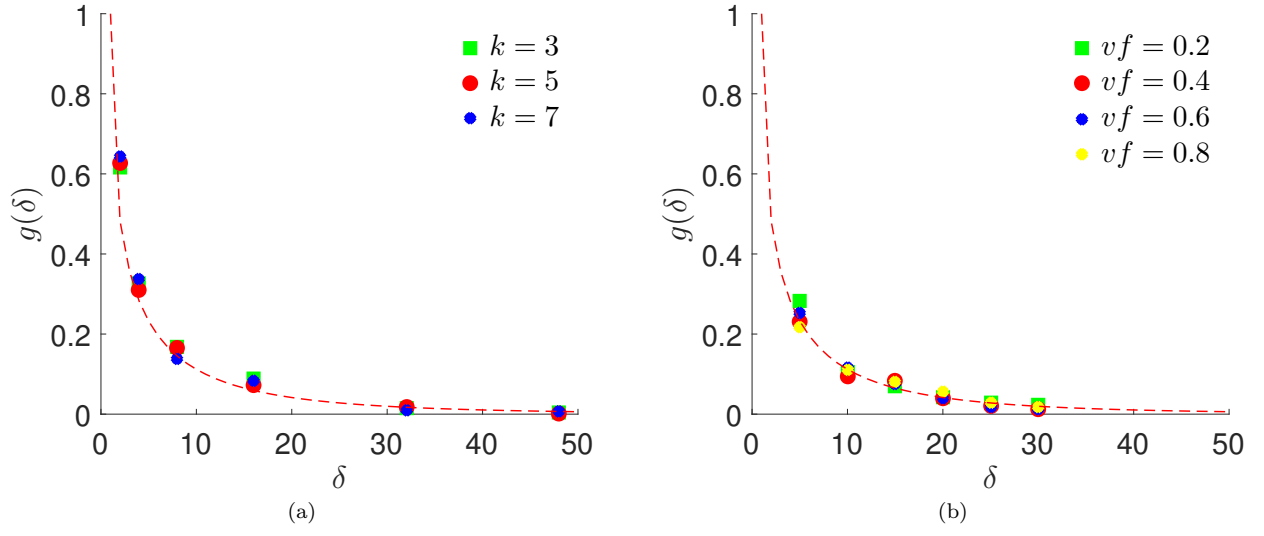
FIG. 7: (Color online) Normalized scaling function $g(\delta)$ as a function of δ showing a good collapse of the stretched exponential function for (a) $v_f = 0.5$ and (b) $k = 7$.

[1] G. W. Milton, The Theory of Composites, Cambridge, UK: Cambridge University Press , 748 (2002).

[2] T. Mura, *Micromechanics of Defects in Solids* (Springer Science & Business Media, 2013).

[3] G. Kristensson and N. Wellander, SIAM Journal on Applied Mathematics **64**, 170 (2003).

[4] A. V. Amirkhizi and S. Nemat-Nasser, Comptes Rendus Mecanique **336**, 24 (2008).

[5] D. R. Smith and J. B. Pendry, JOSA B **23**, 391 (2006).

[6] A. Bensoussan, J.-L. Lions, and G. Papanicolaou, *Asymptotic Analysis for Periodic Structures*, Vol. 374 (American Mathematical Soc., 2011).

[7] A. H. Sihvola, *Electromagnetic Mixing Formulas and Applications*, 47 (IET, 1999).

[8] M. Ostoja-Starzewski, *Microstructural Randomness and Scaling in Mechanics of Materials* (CRC Press, 2007).

[9] M. Ostoja-Starzewski, S. Kale, P. Karimi, A. Malyarenko, B. Raghavan, S. Ranganathan, and J. Zhang, Advances in Applied Mechanics **49**, 111 (2016).

[10] A. Malyarenko and M. Ostoja-Starzewski, *Tensor-Valued Random Fields for Continuum Physics* (Cambridge University Press, 2019).

[11] R. Hill, Journal of the Mechanics and Physics of Solids **11**, 357 (1963).

[12] J. Mandel and P. Dantu, Annales des Ponts et Chausses Paris **6**, 115 (1963).

[13] J. Zhang and M. Ostoja-Starzewski, Proc. R. Soc. A **472**, 20150801 (2016).

[14] M. Ostoja-Starzewski and J. J. Schulte, Phys. Rev. B **54**, 278 (1996).

[15] M. Ostoja-Starzewski, Phys. Rev. B **62**, 2980 (2000).

[16] M. Ostoja-Starzewski and S. Ranganathan, Phys. Rev. B **77**, 214308 (2008).

[17] R. S. Raghavan, B and M. Ostoja-Starzewski, AIP Advances **5**, 017131 (2015).

[18] K. Sab, Eur. J. Mech,. A/Solids , 585 (1992).

[19] J.-M. Jin, *Theory and Computation of Electromagnetic Fields* (John Wiley & Sons, 2011).

[20] C. Huet, Journal of the Mechanics and Physics of Solids **38**, 813 (1990).

[21] E. Kröner, *Statistical Continuum Mechanics*, 92 (Springer, 1972).

[22] *COMSOL Multiphysics® v. 5.3. www.comsol.com. COMSOL AB, Stockholm, Sweden.*

[23] C. Olariu, S. Lasquellec, and C. Brosseau, Journal of Applied Physics **114**, 074104 (2013).

[24] *See Supplemental Material at [URL will be inserted by publisher] for electric flux density norm of 3D two-phase random checkerboard.*